Contents lists available at ScienceDirect

Applied Surface Science

journal homepage: http://ees.elsevier.com

Full Length Article

Highly stable defective TiO_{2-x} with tuned exposed facets induced by fluorine: Impact of surface and bulk properties on selective UV/visible alcohol photo-oxidation

Marianna Bellardita [a,*], Corrado Garlisi [b,c,d], Lütfiye Yildiz Ozer [b,c,d], Anna Maria Venezia [e], Jacinto Sá [f,g], Fikret Mamedov [f], Leonardo Palmisano [a], Giovanni Palmisano [b,c,d]

[a] "Schiavello-Grillone Photocatalysis Group"- Engineering Department, University of Palermo, Viale delle Scienze, 90128 Palermo, Italy
[b] Department of Chemical Engineering, Khalifa University of Science and Technology, P.O. Box 127788 Abu Dhabi, United Arab Emirates
[c] Research and Innovation on CO_2 and H_2 (RICH) Center, Khalifa University of Science and Technology, P.O. Box 127788 Abu Dhabi, United Arab Emirates
[d] Center for Membrane and Advanced Water Technology, Khalifa University of Science and Technology, P.O. Box 135125 Abu Dhabi, United Arab Emirates
[e] ISMN-CNR, Via Ugo la Malfa 153, 90146 Palermo, Italy
[f] Department of Chemistry-Ångström Laboratory, Uppsala University, PO BOX 523, SE-751 20 Uppsala, Sweden
[g] Institute of Physical-Chemistry, Polish Academy of Sciences, Kasprzaka 44/52, 01-224 Warsaw, Poland

ARTICLE INFO

Keywords
Titanium dioxide (TiO_2)
TiO_2 facets
Fluorine effects
Structural and morphological TiO_2 control
2-Propanol and 4-Methoxybenzyl alcohol photo-oxidations
$^{\bullet}OH$ radicals generation rate

ABSTRACT

Titanium dioxide samples were prepared in the presence of different amounts of fluorine via hydrothermal method. It has been found that the presence of fluoride influenced the physico-chemical properties of TiO_2 in various ways as polymorphic form stability, surface hydroxylation, generation of hydroxyl radicals under irradiation and formation of Ti^{3+} centers and oxygen vacancies. The generation rate of $^{\bullet}OH$ radicals was investigated by the photoluminescence technique in the presence of terephthalic acid. X-ray diffractometry indicated that fluorine stabilized the anatase TiO_2. X-Ray photoelectron spectroscopy (XPS) revealed the presence of fluorine on the surface and the shift of the valence band edge towards less negative potentials, electron paramagnetic resonance (EPR) confirmed the formation of Ti^{3+} in the bulk of the photocatalysts, UV–vis spectra showed the extension of the TiO_2 photo-response in the visible light region. 2-Propanol degradation and 4-methoxybenzyl alcohol partial oxidation were studied as probe reactions by using the home prepared powders as photocatalysts. Surprisingly, the photocatalytic activity resulted to be mainly affected by $^{\bullet}OH$ radicals formation ability under irradiation, rather than by the presence of {0 0 1} facets, although it cannot be excluded that the latter could influence the ability to form radicals under irradiation.

1. Introduction

In the last 50 years, heterogeneous photocatalysis has developed in the field of environmental clean-up [1–4], conversion of solar energy and fuels production [5–7], and synthesis of high value added compounds [8–12]. Although a great interest was recently devoted to alternative photocatalysts [13–16], the most used one remains TiO_2 [5,17,18]. Research has been mainly addressed to evaluate strategies to improve the photocatalysts performance because the efficiency of photocatalytic reactions in the presence of TiO_2 has not been found satisfactory for practical applications [19,20]. The main experimental approaches to reduce the charge carrier recombination, to improve their interfacial transfer and to extend the light absorption in the solar/visible region were doping TiO_2 with metal/nonmetal species [21–26], coupling it with other photocatalysts [27–30] or sensitizing its surface with organic compounds [31,32].

A recent strategy consists in preparing TiO_2 with the simultaneous presence of different crystalline facets [33–38] because they possess different coordination environment, and it is reported that the facet with a higher amount of under coordinated fivefold Ti (Ti_{5c}) atoms is more active than that with a lower amount of them [39]. For TiO_2 anatase, in particular, the {1 0 1} facet presents only 50% of Ti_{5c} atoms whilst the {0 0 1} and {1 0 0} ones ca. 100%. Moreover, the most thermodynamically stable facet, and therefore that preferentially obtained during the synthesis process, is the {1 0 1} one. The other main facets, {0 0 1} and {1 0 0}, are less stable and they can be obtained with a certain abundance only under specific experimental conditions [33–35]. In particular, the use of capping agents during the TiO_2 crystallization may be exploited as a way to favour one facet with respect to another, by changing its surface energy and the stability [34,40]. As Yang et al. [33] showed that fluorine adsorption on anatase surface reversed the relative stability of the {1 0 1} and {0 0 1} facets, hydroflu-

* Corresponding author.
E-mail address: marianna.bellardita@unipa.it (M. Bellardita)

https://doi.org/10.1016/j.apsusc.2020.145419
Received 4 November 2019; Received in revised form 3 January 2020; Accepted 14 January 2020
Available online xxx
0169-4332/

oridric acid has been the most used controlling agent [35,36,41–49]. Despite the high number of papers published on this topic, the actual role played in photocatalytic reactions by fluorine present during TiO_2 preparation and/or as a residual species on the photocatalyst surface is not completely clear. In particular, various physico-chemical parameters seem to influence the ratios of the various facets obtained, and the photocatalytic activity appears dependent from various factors having a synergistic effect [43–45,48,49]. Consequently, the multiple role played by fluorine deserves much attention as its presence not only strongly influences the crystallization process addressing the formation of different TiO_2 phases with various facets ratio, depending on the concentration used, but also the surface properties of the photocatalyst [50–52]. The modification of the surface features of the photocatalysts as acidity, hydroxylation degree and enhanced O_2 adsorption [53–57], the different structural variation as the replacement of lattice oxygen with the formation of -Ti-F-Ti- bonds and Ti^{3+} species [51], and the different electronic properties as the longer electron lifetime [45,58] make it hard to compare the photocatalytic activity of samples prepared under various experimental conditions in the presence of a different amount of fluoride ions.

In this work the behaviour of defective TiO_2 samples which were synthesized in the presence of fluorine is reported, and in particular the multiple effects played by this species on the surface physico-chemical and bulk properties which can influence the photoactivity have been investigated.

Differently from a previous paper published by some of us [45], $TiCl_4$, instead of $TiOSO_4$, was the TiO_2 precursor, and a comparison of the photoactivity of the photocatalysts prepared in the presence of various fluorine sources (HF, NaF and NH_4F) was made. Moreover, higher fluorine amounts were used with the aim to increase the formation of the {0 0 1} facet. In this case, as discussed below in the Results and Discussion section, a net difference of the percentage of {0 0 1} facet was found among the various home prepared samples which presented a light blue colour due to the presence of Ti^{3+} species. Notably, previously studied samples did not show significant differences by changing the amount of fluoride used for their preparation. The photocatalysts were characterized by X-ray diffractometry, scanning electron microscopy, transmission electron microscopy, Raman spectroscopy, UV-vis spectrophotometry, photoluminescence spectra, photoinduced hydroxyl radicals' generation, X-ray photoelectron spectroscopy and electron paramagnetic resonance. The photoactivity of the samples was evaluated by carrying out two probe reactions, i.e. 2-propanol degradation and 4-methoxybenzyl alcohol (4-MBA) partial oxidation in gas-solid and liquid-solid systems, respectively. It is worth noticing that the last reaction was carried out not only under UV but also under simulated solar light irradiation. The same probe reactions reported in a previous work by some of us [45] have been performed to try to understand whether the presence of $^{\bullet}OH$ radicals, whose generation was studied by means of photoluminescence spectra, influenced the photocatalytic activity more than the percentage of the {0 0 1} facets present in the various samples.

2. Experimental

2.1. Materials

Titanium tetrachloride (98% Fluka), hydrochloric acid (36.5–38.0% Sigma-Aldrich), hydrofluoric acid (48% w/w Sigma-Aldrich), sodium fluoride (≥99% Sigma-Aldrich), ammonium fluoride (>98% Sigma-Aldrich), 4-methoxybenzyl alcohol (>98% Sigma-Aldrich), 4-methoxybenzaldehyde, (98% Sigma-Aldrich) and 2-propanol (99.8% Sigma-Aldrich), were used as starting materials and reagents.

2.2. Samples preparation

5 mL of $TiCl_4$ were added dropwise to 160 mL of distilled water and 80 mL of HCl under continuous stirring in a Teflon vessel. After the $TiCl_4$ hydrolysis, different amounts of hydrofluoric acid were added to the obtained solution. Some samples were prepared by adding NaF or NH_4F instead of HF. The solution was treated in Pyrex closed bottles at 100 °C for 48 h or in a stainless-steel autoclave at 200 °C for 24 h. After that, the precipitate was recovered, washed three times with distilled water and then dried at 70 °C. The powders were labeled as F/Ti = x, where x represents the molar F/Ti ratio. The abbreviations b and auto indicate the thermal treatment in a closed bottle or in an autoclave, respectively.

2.3. Samples characterization

X-ray diffraction patterns (XRD) were recorded by using a Bruker D8 Advance diffratometer with Cu Kα radiation (k = 1.5406 Å) at 40 kV and 40 mA.

X-ray peak broadening analysis was used to evaluate the crystalline sizes and lattice strain by the Williamson-Hall (W-H) analysis [59].

Raman spectra were recorded with a Witec Alpha 300R Raman spectrometer equipped with a 532 nm diode laser having a power of 75 mW.

Scanning electron microscopy (SEM, FEI Nova NanoSEM) observations were used to investigate the catalyst morphology and the percentage of exposed {0 0 1} facets according to method reported in other works [60,61].

The diffuse reflectance spectra (DRS) were recorded by using a Shimadzu UV-2401 PC spectrophotometer, with $BaSO_4$ as the reference material. Band gap values were determined by plotting the modified Kubelka-Munk function, $[F(R'_{\infty})h\nu]^{1/2}$, versus the energy of the exciting light.

Transmission electron microscopy (TEM) analyses were performed by using FEI Titan and Tecnai microscopes at 200 kV. TEM samples were obtained by the following procedure: (i) preparation of suspension consisting of ca. 1 g L^{-1} of the catalyst in 2-propanol; (ii) treatment by ultrasound for 5 min; (iii) deposition of 2 μL of the mixture onto a Forvar/Carbon 300- mesh Cu grid (purchased from Tedpella); (iv) evaporation of the solvent at room temperature.

Photoluminescence (PL) emission spectra of dry catalysts were recorded using a Perkin Elmer LS-55 Fluorescence Spectrometer. The excitation wavelength was 300 nm.

The generation of $^{\bullet}OH$ radicals was detected by PL analysis using terephtalic acid (TA) as the probe molecule. Due to the reaction with $^{\bullet}OH$ radicals, TA generates 2-hydroxyterephthalic acid (TAOH), which shows the maximum PL signal around 421 nm. For this test, 5×10^{-4} mol/L of TA were diluted in a basic solution containing 2.17×10^{-3} mol/L of NaOH. Then 25 mg of catalyst were added to 25 mL of TA solution under magnetic stirring. A 16.2 W LED lamp was used as the light source. The radiation emission of this lamp ranged between 360 and 370 nm (model 5050 FPC LED strips, with 60 LED strips per meter). The radiation intensity reaching the surface of the suspension was 4.70 W m^{-2} in the 315–400 nm range (measured with a radiometer Delta Ohm 9721 and the matching probe). Sampling was carried out every 3 min for a total of 15 min. Solution after filtration through a 0.2 μm PTFE filter was analysed by the same fluorescence spectrometer mentioned above.

X-ray photoelectron spectroscopy (XPS) spectra were acquired with a VG Microtech ESCA 3000 Multilab, equipped with a dual Mg/Al anode. The spectra were recorded by using the Al Kα source (1486.6 eV) run at 14 kV and 15 mA. Survey spectra and individual peak regions were obtained at 50 eV and 20 eV pass energy respectively. The pow-

dered samples were mounted on a double-sided adhesive tape. All the binding energies were calibrated with respect to the C 1 s peak energy set at 285.1 eV, arising from adventitious carbon. Analyses of the peaks were performed with CasaXPS software. Atomic concentrations were calculated from peak intensity using the sensitivity factors provided by the software. The binding energy values were quoted with a precision of ±0.15 eV and the atomic percentage with a precision of ±10%.

Electron paramagnetic resonance (EPR) measurements were performed with EMX micro spectrometer (Bruker BioSpin GmbH) equipped with an EMX-premium bridge and an ER4119HS resonant cavity. For the low temperature measurements ESR 900 cryostat and ITC 503 temperature controller (Oxfords Instruments, UK) were used. Measurement conditions were: microwave frequency 9.38 GHz, microwave power 50 μW, modulation amplitude 5 G, temperature 20 K. Powder samples were placed in glass capillaries and frozen at liquid N_2 before the measurements.

2.4. Photoreactivity experiments

2.4.1. 2-propanol oxidation

The gas-phase oxidation of 2-propanol was carried out in a cylindrical Pyrex batch photoreactor (volume 130 mL). 0.3 g of the powder was placed inside the reactor. O_2 was fluxed under irradiation to clean the catalyst surface. Subsequently, 2 μL of 2-propanol (concentration 200 μM) were injected into the reactor and the lamp was switched on. A UV 400 W medium pressure Hg lamp placed on the top of the photoreactor (irradiance reaching the catalyst 1.6 mW cm^{-2}) was used as the irradiation source. Gas sampling was done at fixed time interval, and analyses were performed by a Shimadzu GC 2010 gas chromatograph equipped with a Phenomenex Zebron Wax-Plus column and a FID detector. CO_2 was quantified by a HP 6890 Series GC System equipped with a TCD detector and a packed GC 60/80 CarboxenTM-1000 column.

2.4.2. 4-Methoxybenzyl alcohol partial oxidation

The photocatalytic liquid phase partial oxidation of 4-Methoxybenzyl alcohol (4-MBA) was carried out in a Pyrex cylindrical reactor containing 150 mL of 0.5 mM aqueous solution of the substrate. The reactor was irradiated by a 125 W medium pressure lamp (radiant power ca. 120 W m^{-2} in the range 315–400 nm) or by a 100 W halogen lamp (radiant power 2000 W m^{-2} and ca. 0.5 W m^{-2} in the 450–750 nm and 315–400 nm ranges, respectively). The runs lasted 4 h and fixed dispersion amounts were withdrawn at determined time interval. Analyses of the solutions obtained by filtration with 0.2 μm membranes (PTFE, Watman) were carried out by means of a Beckman Coulter HPLC equipped with a Phenomenex Kinetex 5 mm C18 100A column (4.6 mm × 150 mm) to measure the concentration both of the substrate and the formed products. A 20:80 v/v mixture of acetonitrile and 13 mM trifluoroacetic acid aqueous solution was used as the eluent.

3. Results and discussion

Different TiO_2 samples were prepared with the aim to investigate the influence of fluorine presence during the crystallization of the powders on their structural, surface and photocatalytic properties. Initially, samples were prepared by using high molar F/Ti ratios because in a previous work [45] powders synthesized in the presence of small amounts of fluorine showed no large differences in the percentage of {0 0 1} facet. In fact, it is reported in literature that well oriented powders were obtained in the presence of higher fluorine amounts [41,52,53]. Nevertheless, in the present work no solid formation was observed for F/Ti ≥ 4 after the thermal treatment starting from two different TiO_2 ($TiCl_4$ and $TiOSO_4$) and fluorine (NaF, HF) precursors, while a very low TiO_2 amount crystallized when F/Ti = 3; for this reason only samples with F/Ti ≤ 3 were prepared. The presence of fluorine seems to hinder the TiO_2 crystallization.

$TiCl_4$ was chosen as the TiO_2 precursor because it allows to obtain different TiO_2 polymorphs by changing only the experimental conditions [62,63].

The samples prepared at 100 °C were white, while those obtained at 200 °C were light blue coloured and the colour intensity was higher for the samples with the lower F/Ti ratios.

Fig. 1 compares the diffractograms of samples synthesized at 100 °C in the presence of two different fluoride ion (HF and NaF) precursors with that of a sample without fluorine. A commercial anatase TiO_2 (Merck) was chosen as reference as it was not possible to obtain an anatase sample under the same experimental conditions in the absence of fluoride ions. The pristine TiO_2 consisted, in fact, of a brookite/rutile mixture [62] whilst all of the samples containing fluorine, regardless of the precursor, consisted of pure anatase. The result suggests that fluoride ions inhibit the crystallization of rutile and brookite, favouring the formation of pure anatase. The above results are in accordance with literature. Indeed, Yu et al. [50] prepared F^--doped TiO_2 samples by hydrolysis of titanium tetraisopropoxide in NH_4F-H_2O solution, and the disappearance of brookite was noticed as the amount of NH_4F increased. Moreover, rutile disappeared from anatase/rutile mixtures when fluorine was added during the TiO_2 synthesis and this finding was attributed to a reduction of surface defects [51]. No peaks associated with fluorine species were observed for all of the samples, even for the highest fluorine quantities. Moreover, for the main anatase (1 0 1) peak a slight shift to a lower angle compared to commercial bare TiO_2 can be noticed in Fig. 1B in the presence of fluorine for all of the home prepared samples. The shift can be attributed to the substitution of O^{2-} ions with F^- ions with the consequent modification of the crystal lattice [64,65]. Similar behaviour was observed for all of the other samples containing fluorine (Fig. S1 and S2). It is not easy to explain the random variation observed, although it can be tentatively attributed to the different fluorine precursors used.

The samples prepared in autoclave at 200 °C consisted of pure anatase for the highest fluorine amounts, whilst traces of rutile are visible for the lowest fluorine amount (Fig. 2). Moreover, in this case a slight shift towards lower Bragg angles can be observed by considering the enlargement of the (1 0 1) peak (Fig. S1).

The presence of fluorine into TiO_2 lattice was indirectly confirmed by the differences of the cell parameters in comparison to those of the commercial Merck (Table 1). In particular, lattice constants *a* and *c* increase in the presence of fluorine, although the absence of a monotone trend with the increase of its amount. The only exception was the sample F/Ti = 0.25, and this finding could be explained by the contemporary presence of anatase and rutile. In addition, higher strain values were calculated for the samples prepared in the presence of fluorine that were due to formation of defects. Generally, a high lattice strain is due to the presence of an excess number of atoms and defects on the amorphous grain boundary [59]. The different values can be due the different fluorine amounts. Furthermore, in accordance to literature data, an increase in crystallinity was observed with the amount of fluorine.

For the samples prepared at 100 °C, the crystallite size of the different samples (**Φ**) ranges from 45 to 135 nm and it increases with the amount of fluorine (Table 1), while for the samples obtained at 200 °C it varies in a non-linear way with the fluorine amount, regardless of the precursor used.

Fig. 3 shows the Raman spectra recorded for the samples synthesized by a hydrothermal treatment at 200 °C in the presence of different HF amounts. The peaks at 144, 394, 514 and 635 nm^{-1} are due to the characteristic E_g, B_{1g}, A_{1g} and E_g anatase modes, respectively; for the sample F/Ti = 0.25 the bands related to rutile can be observed only by enlarging the Fig. 3. Differently from previous work [45],

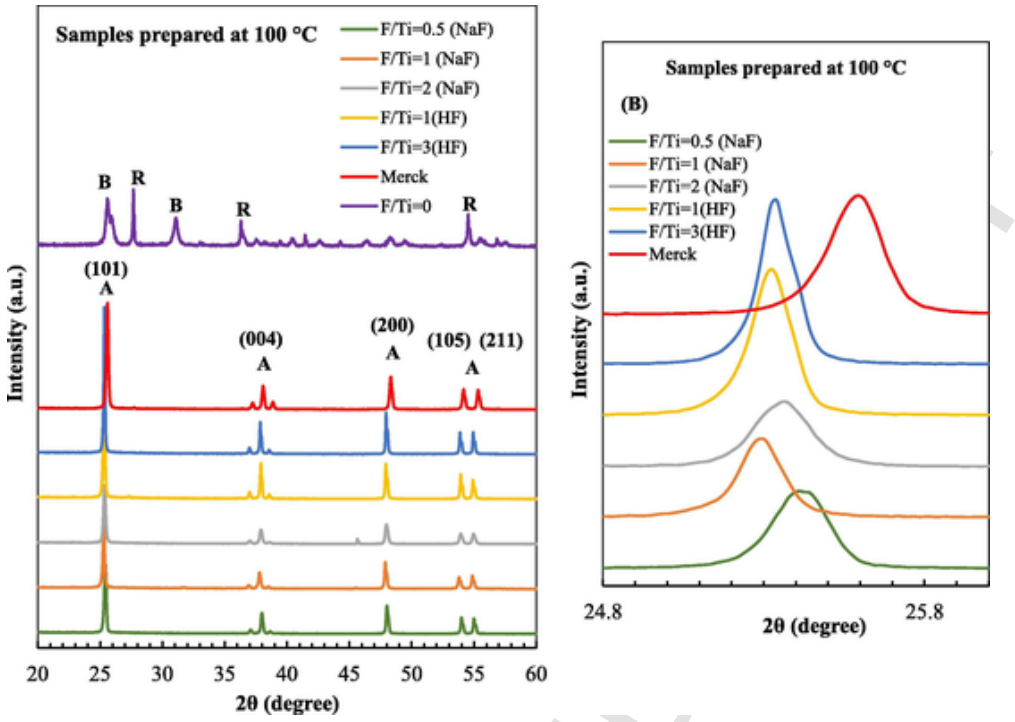

Fig. 1. (A) XRD patterns of the samples prepared in the presence of fluoride ions by thermal treatment at 100 °C. A = Anatase, B = Brookite, R = Rutile; (B) enlargement of the anatase (1 0 1) peak.

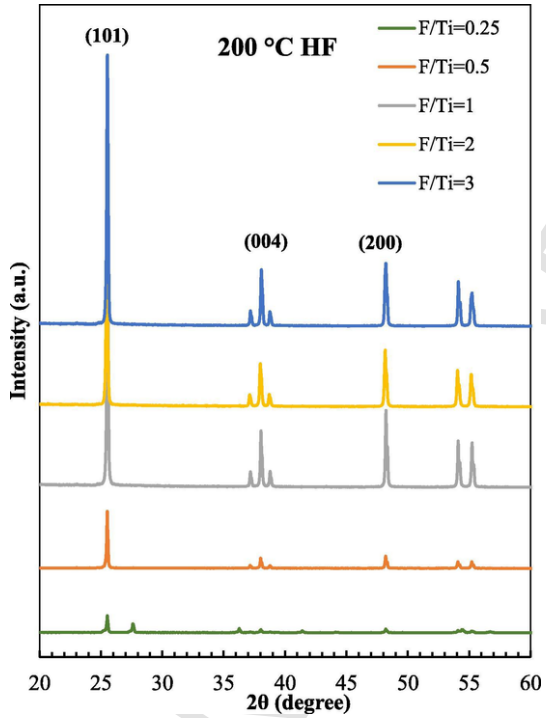

Fig. 2. XRD patterns of the samples prepared in the presence of HF by thermal treatment at 200 °C.

a slight shift to higher frequency of the maximum of the peak at 144 nm^{-1} is noticed (Fig. 3B) for the homemade samples prepared in the presence of fluorine with respect to the commercial TiO_2. This finding indicates the presence of oxygen vacancies related to the presence of Ti^{3+}, as reported in the literature [51,66,67]. In addition, also the broadening of the peak is attributable to the presence of oxygen defects [59].

Generally, the TiO_2 UV–vis absorption spectrum is not affected by adsorbed fluoride on the surface [65], while an enhancement of visible light absorption occurs when fluoride enters the lattice [68]. An increase of absorption in the region from 400 nm up to 800 nm with respect to Merck is evident for all of the samples treated at 200 °C in the presence of HF (Fig. 4), especially for F/Ti = 0.25, in accordance with the blue coloration of the powders, differently from the samples previous prepared [45]. While commercial stoichiometric TiO_2 adsorbs only in the UV light region, the shape of spectra of prepared F-doped photocatalysts is typical of non-stoichiometric TiO_2 with oxygen vacancies and Ti^{3+} centres [67]. The enhanced absorption in the visible and near-infrared region is consistent with the slight blue colour of the prepared powders. The spectra of the catalysts heated at 100 °C (not reported for the sake of brevity) are practically the same as that of TiO_2 Merck. The replacement of O^{2-} ions by F^- ones resulted in a charge imbalance with formation of Ti^{3+} centres. These centres are responsible for the existence of a typical band below the conduction band explaining the enhanced absorption in the visible range. The band gap values (Table 1) decreased with respect to Merck for the samples prepared at 200 °C, and the lowest value was obtained for F/Ti = 0.25, due both to oxygen vacancies (evidenced by the colour) and to the contemporary presence of anatase and small amounts of rutile.

Photoluminescence (PL) spectra give information on the recombination of e^-/h^+ pair, lattice defects, and oxygen vacancies. It is difficult to compare these spectra with those reported in the literature because the experimental conditions for the preparation of the samples are very different. In general, the lower the recombination rate the lower the PL intensity, whilst the higher the content of defects and/or oxygen vacancies the stronger the signal. In Fig. 5 the spectra of the samples prepared in the presence of the different amounts of fluorine are reported; all of the catalysts presented emission spectra of similar shape with similar PL signals at different molar F/Ti ratios. In particular the following main peaks can be observed: a weak UV shoulder at 382

Table 1
Cell parameters, lattice strain, crystallite size and band-gap value of the different samples.

Sample	Cell parameters		Volume (Å^3)	η (Strain) × 10^{-3}	Φ [a] (nm)	Band-gap (eV)
	a = b (Å)	c (Å)				
F/Ti = 1 (HF) b	3.7970	9.501	136.97	4.4	102	3.15
F/Ti = 3 (HF) b	3.7955	9.514	137.06	4.8	135	3.20
F/Ti = 0.5 (NaF) b	3.7930	9.497	136.67	0.1	45	3.24
F/Ti = 1 (NaF) b	3.7992	9.526	137.49	3.6	76	3.24
F/Ti = 2 (NaF) b	3.7960	9.509	137.01	3.9	59	3.26
F/Ti = 3 (NaF) b	3.778	9.486	135.43	2.6	87	3.10
F/Ti = 0.25 (HF) auto	3.77	9.42	133.89	5.3	222	2.98
F/Ti = 0.5 (HF) auto	3.786	9.495	136.1	2.0	85	3.13
F/Ti = 1 (HF) auto	3.7790	9.487	135.45	2.1	53	3.15
F/Ti = 2 (HF) auto	3.7810	9.493	135.71	4.9	106	3.14
F/Ti = 3 (HF) auto	3.7820	9.489	135.75	3.8	101	3.02
F/Ti = 1 (HF) auto 43 h	3.7760	9.485	135.25	0.5	66	3.06
F/Ti = 3 (NaF) auto	3.7800	9.489	135.59	4.0	106	3.13
F/Ti = 3 (NH_4F) auto	3.7820	9.530	136.28	4.9	91	3.06
Merck	3.7730	9.483	134.97	2.8	58	3.26

[a] Calculated by the Williams Hall method.

nm due to the e^-/h^+ in the conduction and valence band of TiO_2, and a peak at 420 nm that can be attributed to the self-trapped excitons localized in octahedral TiO_6 [69,70]. The intensity of this signal increases when moving from F/Ti = 1 to F/Ti = 3, indicating a higher charge recombination with increasing the fluorine amount. On the other hand, F/Ti = 0.25 and F/Ti = 0.5 show their main emission peak between those of F/Ti = 1 and F/Ti = 2. Emission at lower energy, i.e. 456, 483 and 540 nm can be assigned to excitonic PL deriving from lattice defects such as oxygen vacancies, interstitial sites of Ti atoms and impurities [70-72]. However, these signals cannot be related straightforwardly to the separation of photogenerated carriers [69].

The analysis of $^{\bullet}$OH radicals was carried out by PL technique using TA as a probe molecule. The PL emission spectra of TA solution excited at 315 nm were recorded every 3 min of UV irradiation. The gradual increase in PL intensity at 421 nm was observed with increasing irradiation time, indicating the formation of TAOH following the reaction of TA with $^{\bullet}$OH radicals generated on the surface of the photocatalyst (Fig. 6A) [73–75]. The PL intensity increased linearly versus time under UV illumination, proving that the generation of $^{\bullet}$OH radicals is a zero-order reaction with respect to TAOH (Fig. 6B). The PL intensity at 421 nm per unit time, i.e. the slope of the plots in Fig. 4B, can thus be used to estimate the formation rate of $^{\bullet}$OH radicals. Results are summarized in Fig. 6C, comparing the slopes of PL intensity for the various photocatalysts. It can be inferred that *(i)* the amount of $^{\bullet}$OH radicals differs for different samples under similar conditions, *(ii)* F/Ti = 0.5 is the sample with the largest amount of $^{\bullet}$OH radicals whose formation is increasingly suppressed with increasing F/Ti ratios above 0.5, *(iii)* the trend is consistent with the results derived from photocatalytic tests (Fig. 6), indicating that the $^{\bullet}$OH radicals are the main active species involved in 4-MBA degradation.

SEM images in Fig. 7 display the morphology of F/Ti = 0.5 and F/Ti = 3. The percentage of exposed facets was computed from the size and geometry of anatase crystals according to the method reported by Zu et al. and Hu et al. [60,61]. In particular, one can note the presence of tetragonal bypiramids which consist of eight lateral [73] facets and two {0 0 1} facets capping the vertexes of the structure, resulting in decahedral crystals (Fig.S3). It can be observed an increase in the average size of these structures when going from F/Ti = 0.5 to F/Ti = 3, denoting a larger crystallites size with increasing fluorine amount in accord with XRD analyses. In addition, an enhanced percentage of exposed {0 0 1} was found at higher F/Ti ratios, as summarized in Table 2. This trend suggests that higher concentrations of HF during the catalyst synthesis favours the {0 0 1} facets, while a too low fluorine concentration causes a marked aggregation of TiO_2 crystals with reduced amount of {0 0 1} facets, in accordance with a previous paper where low fluorine amounts were used [45]. As a consequence, it is impossible to determine the percentage of these facets in F/Ti = 0.25 by means of the methods used at higher F/Ti ratios. In F/Ti = 0.25, the growth of {0 0 1} facets may be inhibited by the lack of a significant amount of F^-, whose chemisorption on the TiO_2 crystal plays crucial role in delaying agglomeration phenomena, thus ensuring a higher average size [60]. Notably, small deposits were observed on the {0 0 1} facet of the catalyst prepared with the highest fluorine amount (i.e. F/Ti = 3), which along with big decahedral crystals, also exhibited elongated crystals of irregular shape (SEM and TEM images, Fig. S4), not found at lower fluorine content.

Fig. 8 shows TEM images of F/Ti = 0.25 and F/Ti = 0.5. In addition to the well-faceted decahedral crystals, further polygonal shapes with a wide size distribution were observed in the different samples (Fig. 8A). TEM analysis confirmed the increase in the average size of the decahedral crystals with increasing F/Ti ratio and the appearance of elongated crystals at F/Ti = 3 (Fig. S4B). At high resolution, the lattice fringes of the TiO_2 particles allowed the identification of the lattice spacings and the indexing of the corresponding crystal planes. Fig. 8B and C display HRTEM images of two characteristic anatase particles in the sample F/Ti = 0.5. In one case (i.e. decahedral crystals), the lattice spacing of 0.189 nm was assigned to (2 0 0) plane of anatase TiO_2 (Fig. 8B), while in the other the lattice spacing of 0.238 nm was attributed to (0 0 4) plane of the same phase (Fig. 8C).

XPS measurements were carried out to investigate the chemical states of Ti, F and O; the results are reported in Table 3. Chlorine cannot be incorporated as doping species into TiO_2 probably because Cl^- presents a larger ionic radius than fluoride (181 versus 133 pm), and moreover it cannot be considered a suitable base to replace basic surface OH groups. F/Ti = 0.25 sample was chosen as it was the most coloured one, with a possible high defects concentration. Titanium Ti 2p spectrum was characterized by the two spin orbit components Ti $2p_{3/2}$ and Ti $2p_{1/2}$, separated by 5.7 eV [76-78]. The binding energy of the Ti $2p_{3/2}$, as listed in Table 3, was at ca. 459 eV and it is attributed to Ti^{4+} [79]. As shown in Fig. 9A, there is no evidence of Ti^{3+} component, however, the light blue colour of the sample is an indication of the presence of Ti^{3+} species [67]. From these results it can be inferred that Ti^{4+} species are prevalently present on the TiO_2 surface, whilst the Ti^{3+} ones are formed in the bulk giving rise to a non-stoichiometric TiO_{2-x} core. The thickness of the stoichiometric TiO_2 shell is therefore greater than the XPS detection limit, normally less than 10 nm.

The O 1 s spectra mainly consist of by two components, one at lower binding energy, 530.2 ± 0.2 eV, due to lattice oxygen forming Ti-O bond and the other one at 531.7 ± 0.2 eV that can be attributed to the surface –OH bound to titanium. A third peak at *ca.* 533 eV could be due to oxygen surface defects.

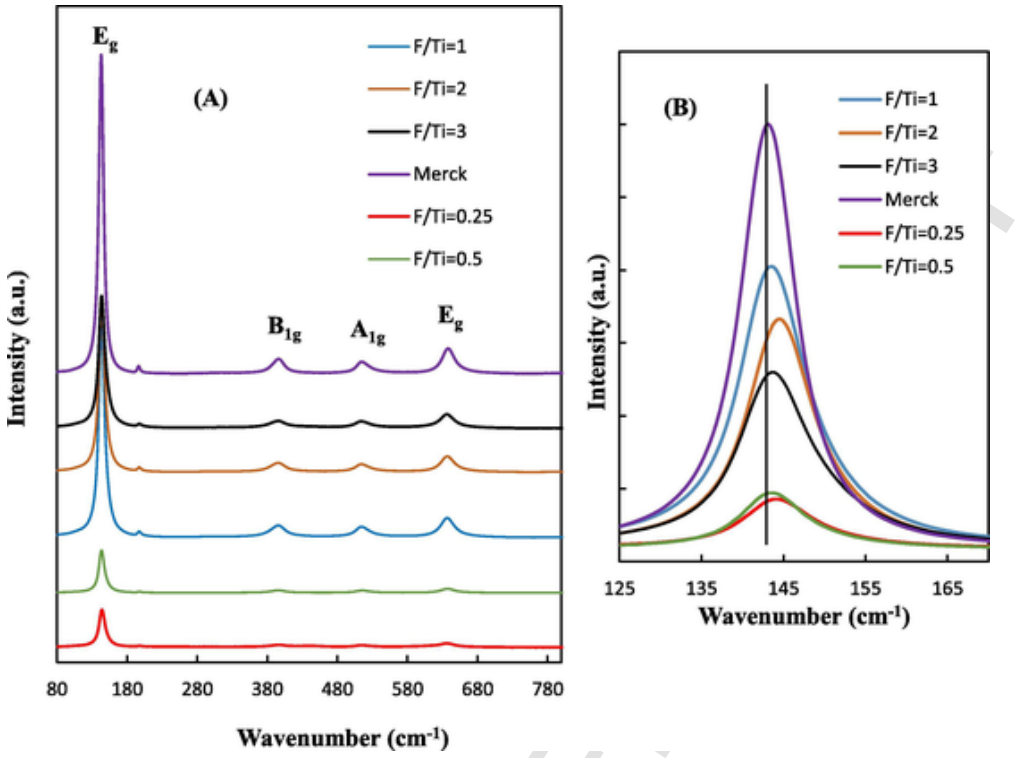

Fig. 3. Raman spectra of the samples prepared at 200 °C in the presence of different HF amounts. Commercial Merck is reported as comparison.

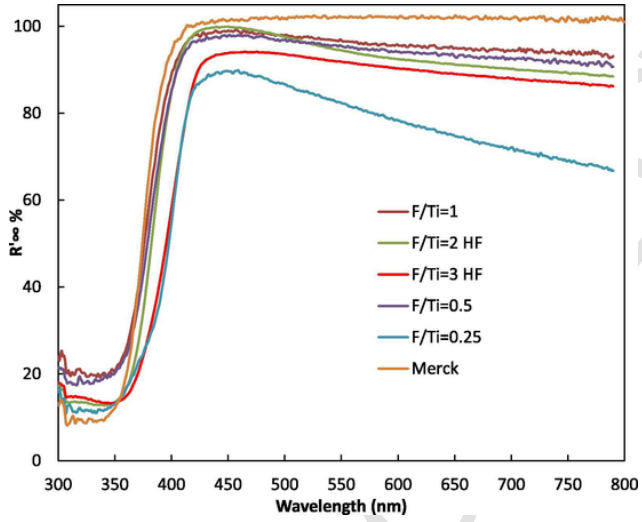

Fig. 4. UV–Vis diffuse reflectance spectra of TiO_2 samples obtained at 200 °C in the presence of different HF amounts compared with commercial anatase.

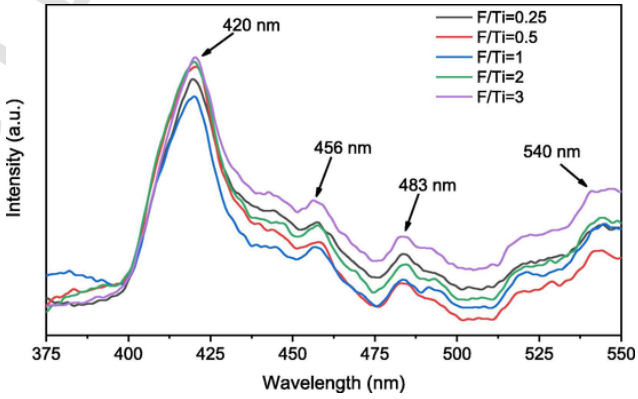

Fig. 5. PL spectra of the photocatalysts (excitation at 300 nm).

The oxygen intensity ratio as Ti-OH/Ti-O of the fluorine containing samples was consistently lower with respect to the commercial TiO_2, confirming the F^- replacement of the –OH groups.

The F 1 s spectra is formed by 2–3 components. As expected, the main component, found at 684.4 eV, is attributed to F^- adsorbed at the surface of the TiO_2 replacing the hydroxyl groups [50,55,57]. The other components at higher binding energies are due to fluoride ions inserted into the TiO_2 lattice which give rise to $TiO_{2-x}F_x$ [56,80,81]. An example of the F1s spectrum is reported in Fig. 9B where the spectra of the sample F/Ti = 0.25 before and after the reaction test are reported. After the test, the component at higher binding energy, attributed to lattice fluorine, increases with respect to that relating to the surface fluorine. In accordance with Wang et al. [64], the physically adsorbed fluorine is removed during the dispersion in water, as evidenced by the decrease of the F/Ti ratio.

The measured F/Ti ratio showed a non-linear trend with the fluorine amount that first increases and then decreases, reaching a maximum in correspondence of the F/Ti = 2. Moreover, the sample with the longest treatment in HF contains the largest amount of fluoride ions.

The XPS valence band spectra of the samples obtained by varying the F/Ti ratio are reported in Fig. 10. All of the spectra contain three main peaks due to the molecular orbitals with contributions from O 2p non-bonding states, π states and σ states represented by I, II, III respectively. The valence band edges (E_g) are obtained by extrapolating the linear portion of the lower energy side of the valence band to the spectral baseline. The commercial sample (Merck) has the most positive value of the valence band potential and, the presence of fluorine shifts this value towards less positive potentials. In particular, the valence band potential decreases by decreasing the F/Ti ratio. The progressive shift of the valence band edge corresponds to the band gap narrowing.

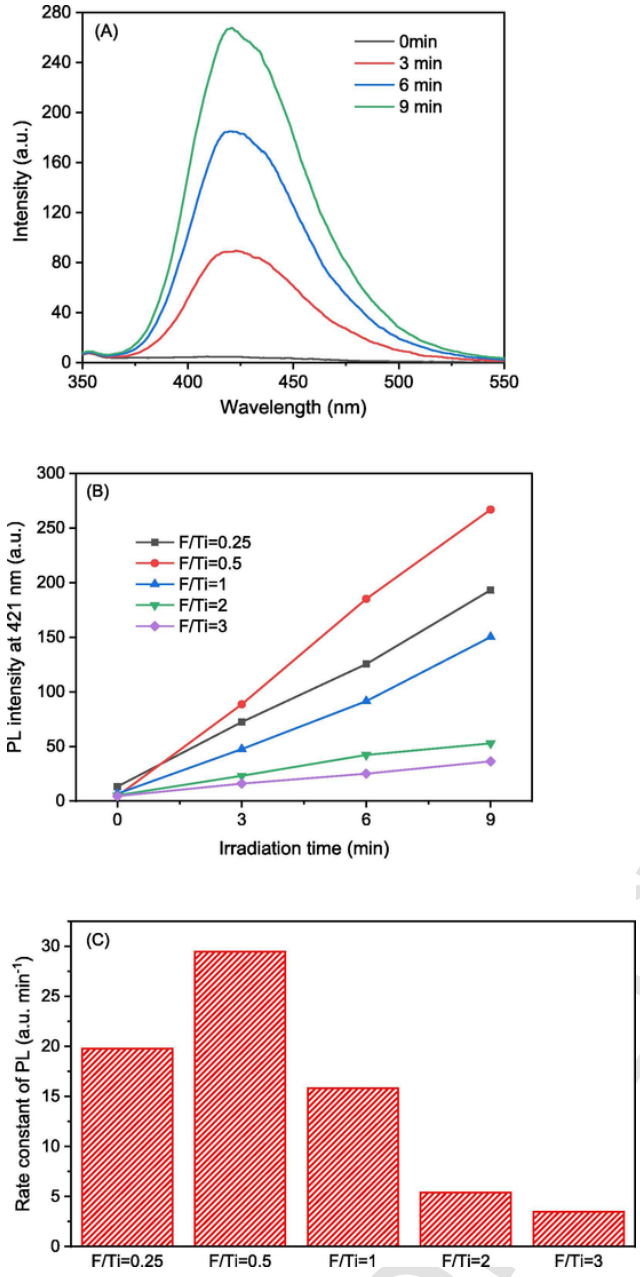

Fig. 6. (A) PL spectra change recorded during UV irradiation of the F/Ti = 0.5 catalyst in a basic solution of TA (excitation at 315 nm). (B) Time dependence of the PL intensity at 421 nm for the different catalysts; (C) Comparison between the corresponding slopes of PL intensity at 421 nm.

Fig. 11 shows EPR measurements performed on the F/T = 0.25 samples. The commercial anatase sample was EPR silent at our measuring conditions indicating absence of any Ti^{3+} related signals (spectrum a). In contrast, F/T = 0.25 sample obtained after hydrolysis and heat treatment, shows EPR signals which can be assigned to Ti^{3+} centres (Fig. 11, spectrum b). Two separate signals can be distinguished: one dominating signal with $g = 1.976$ and $g = 1.1943$ components which can be attributed to the presence of Ti^{3+} in the rutile and a small intensity at $g = 1.993$ component of the Ti^{3+} in the anatase polycrystalline lattice. Similar g values were reported before for these two polymorphs [82]. The small intensity from the anatase (only ⊥ component of the axial signal is visible, see magnified spectrum b) indicates that most of the Ti^{3+} centres are found in the rutile polymorph. It should be noted that both EPR signals (i.e. Ti^{3+} centres) were still present after photocatalytic run (spectrum c).

In Table 4 the results of the gaseous partial oxidation of 2-propanol are reported in terms of 2-propanol initial degradation rate (r_0), acetone selectivity ($S_{acetone}$) and mineralization percentage (CO_2 %). All the runs lasted 4 h and the initial 2-propanol concentration was 200 μM. By comparing the results related to the samples prepared by keeping constant the F/Ti ratio (F/Ti = 1), and changing the synthesis temperature (second and fifth line in Table 4), it could be concluded that the samples obtained at 200 °C showed a higher activity (higher degradation rate and mineralization degree) compared to that prepared at 100 °C. For this reason, and by considering that it was not possible to quantify the percentage of the {0 0 1} facet for these samples, only the photoactivity of the powders prepared in the autoclave was investigated. The initial degradation rate of 2-propanol showed a bell-shaped pattern. The highest value can be observed in the presence of the sample F/Ti = 0.5, whilst the lowest in the presence of the F/Ti = 2. The selectivity to acetone was always quite high reaching 99% with F/Ti = 0.5, on the contrary 2-propanol mineralization degree was low for all of the samples. In Fig. 12 the concentration trend of 2-propanol and acetone is shown as a function of irradiation time. The most active sample was that prepared in autoclave starting from a F/Ti nominal ratio equal to 0.5. In the presence of this sample the largest amount of $^{\bullet}OH$ radicals under irradiation was formed (Fig. 6), and the lowest amount of {0 0 1} facet was found. In this case, therefore, the parameter that most influenced the photoactivity was the quantity of $^{\bullet}OH$ radicals rather than the {0 0 1} facets amount. Moreover, the samples containing more F are less active. It cannot be excluded, however, that the quantity of $^{\bullet}OH$ radicals could depend also on the presence of an optimum amount of {0 0 1} facets in the sample, although a straightforward relation between these factors is not easy to be found.

The results related to the 4-MBA conversion are reported in Fig. 13. Under UV light irradiation (Fig. 13A) the alcohol oxidation was the highest in the presence of the F/Ti = 0.5 sample and then decreased, whilst the selectivity both to the aldehyde and the acid reached the maximum values with the sample F/Ti = 2. The above finding is in accord with the general trend that, during alcohols partial oxidation, the higher the conversion the lower the selectivity [12,83].

Due to the increased absorption in the visible region (Fig. 4), the samples were also tested under simulated solar light irradiation (Fig. 13B). Alcohol conversion was lower than under UV irradiation (due to the low UV photon amount) and the selectivity, also in this case, was higher in the presence of the sample F/Ti = 2. Virtually, no acid was formed under solar light irradiation.

In the case of 4-MBA, the higher amount of $^{\bullet}OH$ radicals and the lower quantity of {0 0 1} facets improved the conversion and reduced the selectivity to aldehyde. In this case, the low amount of $^{\bullet}OH$ radicals, that are highly oxidant species, reduced the total oxidation ability and favoured the partial oxidation.

It is worth pointing out that the Ti^{3+} species were very stable as no colour attenuation was observed after the recovery of the photocatalysts at the end of the photocatalytic runs, both in gaseous or aqueous phase. This finding was also confirmed by EPR measurements.

As it is reported that the presence of Ti^{3+} species in the TiO_2 matrix enhances the hydrogen production under visible light [84], runs in the presence of the sample F/Ti = 0.25 (the most coloured one) were carried out in a closed system under visible light irradiation by using formic acid as the sacrificial agent [6]. After 4 h of irradiation, a formic acid conversion of ca. 50% was measured along with some CO_2 production but no H_2 formation was observed. The oxygen vacancies potential, located below the conduction band edge, is probably more positive than the hydrogen redox potential, inhibiting its formation.

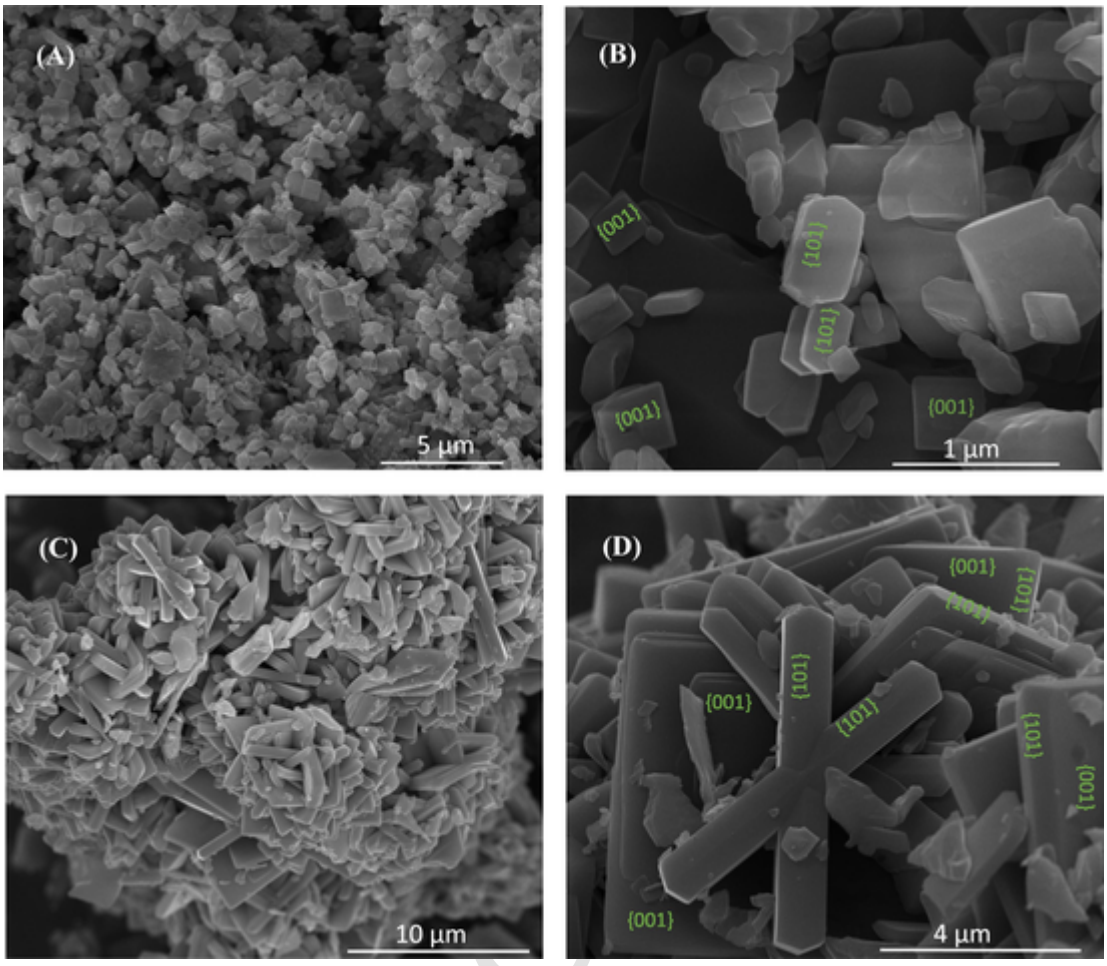

Fig. 7. SEM images of F/Ti = 0.25 (A) and (B) and F/Ti = 3 (C) and (D) at two different magnifications.

Table 2
Percentage of {0 0 1} facet.

Sample	Average {0 0 1} %
F/Ti = 0.25	–
F/Ti = 0.5	19
F/Ti = 1	37
F/Ti = 2	42
F/Ti = 3	48
F/Ti = 1 43 h	34

4. Conclusions

In this work TiO_2 samples containing different amounts of fluorine were synthesized by a hydrothermal method. The presence of fluorine during the photocatalysts crystallization induced the preferential anatase formation, the replacement of TiO_2 surface –OH groups, the increase of the {0 0 1} facet percentage, the generation of high amount of $^{\bullet}OH$ radicals under irradiation, the formation of Ti^{3+} species due to their insertion in the TiO_2 lattice and a shift in the valence band edge. The catalytic properties of these powdered photocatalysts were investigated both in liquid and gaseous regime by following the oxidation of two alcohols used as the probe molecules. The percentage of {0 0 1} facet increased with the fluorine amount whilst the maximum $^{\bullet}OH$ radicals concentration was measured for the samples with the lowest F/Ti ratio. In particular, the F/Ti = 0.5 sample showed to be the best one to achieve the total conversion of the investigated alcohols. The most important parameters which influence the photoactivity were the amount of $^{\bullet}OH$ radicals and the formation of defects. The percentage of the {0 0 1} facet seems to be not very relevant, differently from what reported in many papers [36,39,44,46,47], probably due to the different experimental conditions under which the photocatalysts were prepared. The stable blue colour of the powders suggests that the Ti^{3+} species are located in the bulk and they can migrate to the surface giving rise to energetically favoured sites. EPR measurements confirmed the presence of Ti^{3+} centres. The permanent formation of Ti^{3+} species and oxygen vacancies reduced the electron–hole recombination rate and induce a change in surface charges that was responsible for the high activity of these samples. Moreover, the formation of Ti^{3+} made the samples active under solar light irradiation.

Declaration of Competing Interest

The authors declare that they have no known competing financial interests or personal relationships that could have appeared to influence the work reported in this paper.

Appendix A. Supplementary material

Supplementary data to this article can be found online at https://doi.org/10.1016/j.apsusc.2020.145419.

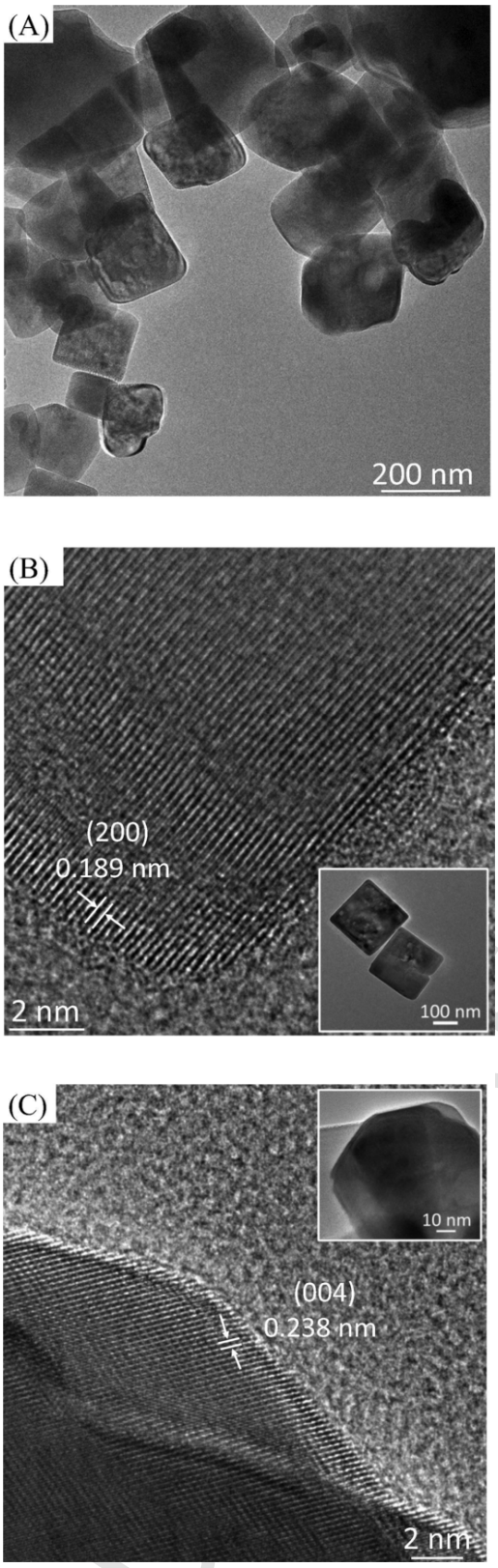

Fig. 8. TEM images of F/Ti = 0.25 (A) and F/Ti = 0.5 (B, C). The insets in (B) and (C) display low magnification images of the particles where the lattice spacings were measured.

Table 3
Summary of XPS results.

Samples	Ti 2p3/2	O1s (%)	F1s (%)	Ti-OH/Ti-O	F/Ti
TiO_2 Merck	459.2	530.1(65) 531.8(21) 532.9(14)	–	0.323	–
F/T = 0.25 used	459.0	530.1(85) 531.6(9) 532.8(4)	684.4(53) 689.2(34) 691.7(13)	0.106	0.09
F/Ti = 0.25	459.1	530.2(92) 531.9(6)	684.5(82) 687.6(9) 691.7(9)	0.065	0.11
F/Ti = 0.5	459.2	530.3(87) 531.5(8) 532.8(3)	684.6(81) 687.9(11) 691.5(8)	0.092	0.12
F/Ti = 1	459.1	530.2(87) 531.7(8) 532.9(3)	684.4(87) 687.7(5) 691.3(7)	0.092	0.21
F/Ti = 1_43h	459.5	530.4 (70) 532.1(17) 533.2(11)	684.9(91) 687.3(9)	0.243	0.43
F/Ti = 2	459.3	530.3(85) 531.8(10) 533.0(4)	684.6(93) 686.9(4) 691.7(3)	0.118	0.3
F/Ti = 3	459.1	530.2(85) 531.7(10) 532.9(4)	684.4(92) 688.9(5) 691.3(3)	0.118	0.2

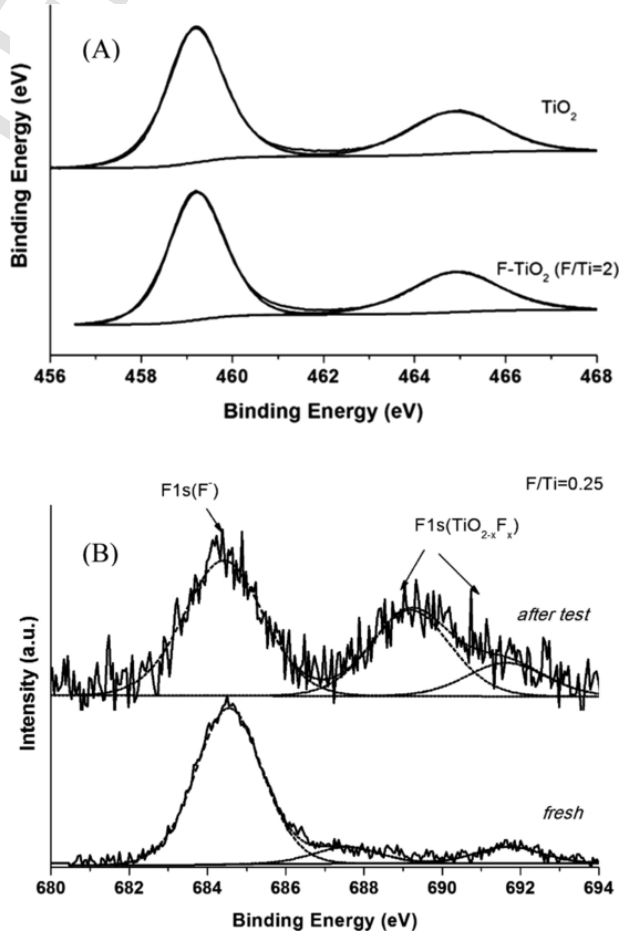

Fig. 9. (A) Ti 2p spectrum of pure TiO_2 and F-doped TiO_2; (B) F1s spectrum of fresh and spent F-TiO_2 (F/Ti = 0.25).

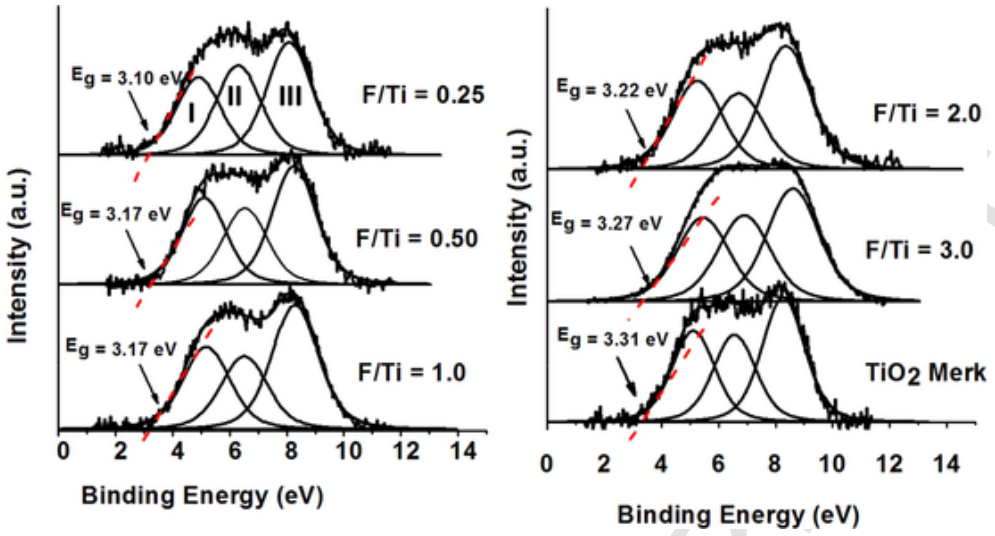

Fig. 10. XPS valence band spectra of the samples with prepared starting from different F/Ti ratios.

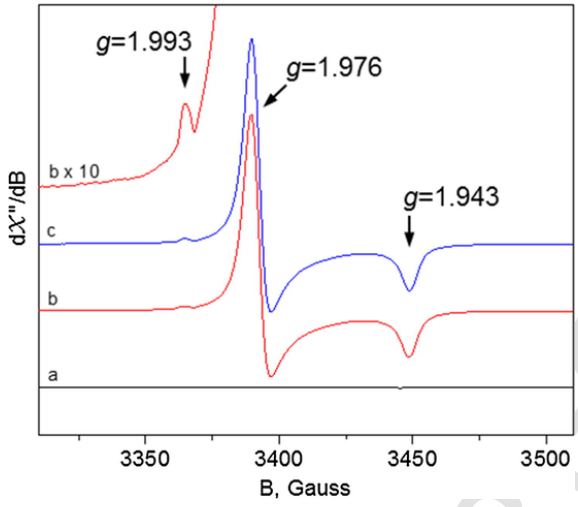

Fig. 11. EPR measurements of the commercial anatase sample (a) and prepared at 200 °C F/Ti = 0.25 samples before (b) and after (c) photocatalytic run. EPR conditions are described in the methods section.

Table 4
Results of the photocatalytic oxidation of 2-propanol in gas phase under UV irradiation. r_0 = initial 2-propanol degradation rate; S = selectivity.

Sample	$r_o \times 10^9$ [mol $L^{-1}s^{-1}$]	$S_{acetone}$ (%)	CO_2 (%)
F/Ti = 1 100 °C	6.7	61	1.5
F/Ti = 0.25 200 °C	18.3	93	1.6
F/Ti = 0.5 200 °C	24.2	99	4.1
F/Ti = 1 200 °C	16.7	55	3.5
F/Ti = 2 200 °C	3.3	92	0.8

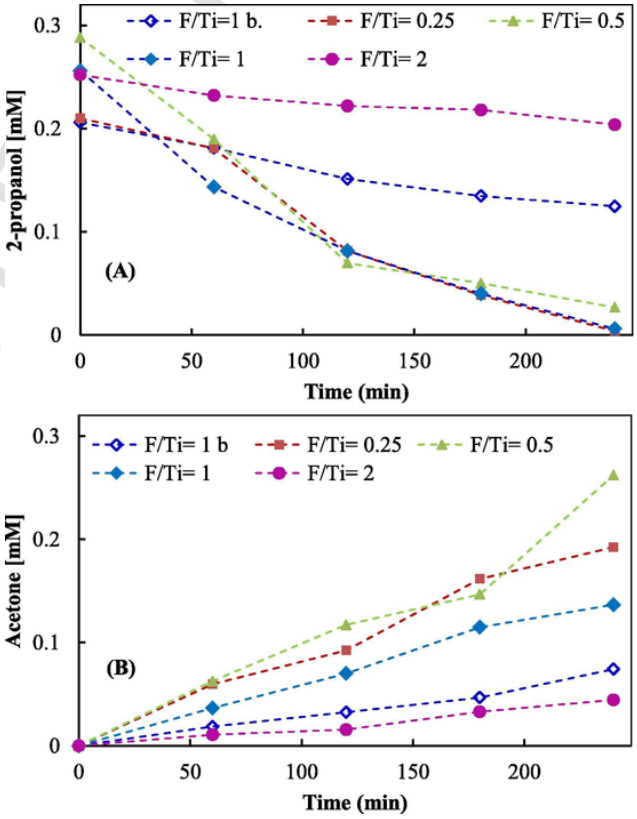

Fig. 12. 2-propanol (A) and acetone (B) concentrations versus irradiation time in the presence of different samples. Photocatalysts amount 0.3 g.

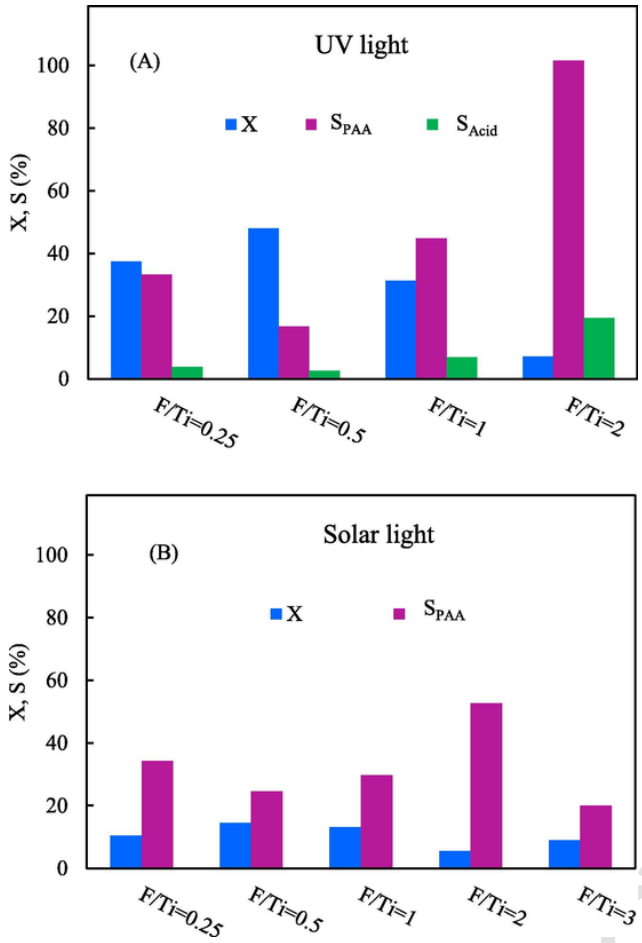

Fig. 13. 4-MBA conversion and selectivity values under UV (A) and simulated solar light (B) irradiation.

References

[1] A.O. Ibhadon, P. Fitzpatrick, Catalysts 3 (2013) 189–218.
[2] J.-M. Herrmann, Catal. Today 53 (1999) 115–129.
[3] S. Ahmed, M.G. Rasul, W.N. Martens, R. Brown, M.A. Hashib, Water Air Soil Pollut. 215 (2011) 3–29.
[4] U.I. Gaya, A.H. Abdullaha, J. Photochem. Photobiol. C 9 (2008) 1–12.
[5] Y. Ma, X. Wang, Y. Jia, X. Chen, H. Han, C. Li, Chem. Rev. 114 (2014) 9987–10043.
[6] M. Bellardita, E. García-López, G. Marcì, G. Nasillo, L. Palmisano, Europ. J. Inorg. Chem. 2018 (2018) 4522–4532.
[7] K. Maeda, K. Domen, J. Phys. Chem. Lett. 1 (2010) 2655–2661.
[8] F. Parrino, M. Bellardita, E.I. García-López, G. Marcì, V. Loddo, L. Palmisano, ACS Catal. 8 (2018) 11191–11225.
[9] N. Corrigan, S. Shanmugam, J. Xu, C. Boyer, Chem. Soc. Rev. 45 (2016) 6165–6212.
[10] J. Kou, C. Lu, J. Wang, Y. Chen, Z. Xu, R.S. Varma, Chem. Rev. 117 (2017) 1445–1514.
[11] M. Bellardita, E.I. García-López, G. Marcì, I. Krivtsov, J.R. García, L. Palmisano, Appl. Catal. B 220 (2018) 222–233.
[12] L. Palmisano, V. Augugliaro, M. Bellardita, A. Di Paola, E. García López, V. Loddo, G. Marcì, G. Palmisano, S. Yurdakal, ChemSusChem 4 (2011) 1431–1438.
[13] A. Di Paola, E. García-López, G. Marcì, L. Palmisano, J. Hazard. Mater. 211–212 (2012) 3–29.
[14] M.D. Hernández-Alonso, F. Fresno, S. Suárez, J.M. Coronado, Energy Environ. Sci. 2 (2009) 1231–1257.
[15] A. Nikokavoura, C. Trapalis, Appl. Surf. Sci. 391 (2017) 149–174.
[16] X. Li, J. Yu, S. Wageh, A.A. Al-Ghamdi, J. Xie, Small 12 (2016) 6640–6696.
[17] K. Nakata, A. Fujishima, J. Photochem. Photobiol. C 13 (2012) 169–189.
[18] A. Fujishima, T.N. Rao, D.A. Tryk, J. Photochem. Photobiol. C 1 (2000) 1–21.
[19] H. Dong, G. Zeng, L. Tang, C. Fan, C. Zhang, X. He, Y. He, Water Res. 9 (2015) 128–146.
[20] S.G. Kumar, L.G. Devi, J. Phys. Chem. A 115 (2011) 13211–13241.
[21] D. Dvoranová, V. Brezová, M. Mazúr, M.A. Malati, Appl. Catal. B 37 (2002) 91–105.
[22] A. Di Paola, E. Garcıa-Lopez, S. Ikeda, O.B. MarcıG, L. Palmisano, Catal. Today 75 (2002) 87–93.
[23] J. Choi, H. Park, M.R. Hoffmann, J. Phys. Chem. C 114 (2010) 783–792.
[24] L. Gomathi Devi, R. Kavitha, Appl. Catal. B 140–141 (2013) 559–587.
[25] S.A. Bakar, C. Ribeiro, J. Photochem. Photobiol. C 27 (2016) 1–29.
[26] R. Amadelli, L. Samiolo, M. Borsa, M. Bellardita, L. Palmisano, Catal. Today 206 (2013) 19–25.
[27] R. Fiorenza, M. Bellardita, L. D'Urso, G. Compagnini, L. Palmisano, Catalysts 6 (2016) 121.
[28] G. Longo, F. Fresno, S. Gross, U.L. Štangar, Environ. Sci. Pollut. Res. 21 (2014) 11189–11197.
[29] D.P. Kumar, M.V. Shankar, M.M. Kumari, G. Sadanandam, B. Srinivas, V. Durgakumari, Chem. Commun. 49 (2013) 9443–9445.
[30] L. Chen, X. Zhou, B. Jin, J. Luo, X. Xu, L. Zhang, Y. Hong, Int. J. Hydrogen Energ. 41 (2016) 7292–7300.
[31] W.M. Campbell, A.K. Burrell, D.L. Officer, K.W. Jolley, Coordin. Chem. Rev. 248 (2004) 1363–1379.
[32] T. Wu, G. Liu, J. Zhao, H. Hidaka, N. Serpone, J. Phys. Chem. B 102 (1998) 5845–5851.
[33] H.G. Yang, C.H. Sun, S.Z. Qiao, J. Zou, G. Liu, S.C. Smith, H.M. Cheng, G.Q. Lu, Nature 453 (2008) 638–642.
[34] G. Liu, J.C. Yu, G.Q. Lu, H.-M. Cheng, Chem. Commun. 47 (2011) 6763–6783.
[35] G. Liu, H.G. Yang, J. Pan, Y.Q. Yang, G.Q. Lu, H.M. Cheng, Chem. Rev. 114 (2014) 9559–9612.
[36] X. Han, Q. Kuang, M. Jin, Z. Xie, L. Zheng, J. Am. Chem. Soc. 131 (2009) 3152–3153.
[37] J. Yu, J. Low, W. Xiao, P. Zhou, M. Jaroniec, J. Am. Chem. Soc. 136 (2014) 8839–8842.
[38] T.R. Gordon, M. Cargnello, T. Paik, F. Mangolini, R.T. Weber, P. Fornasiero, C.B. Murray, J. Am. Chem. Soc. 134 (2012) 6751–6761.
[39] X.Q. Gong, A. Selloni, J. Phys. Chem. B 109 (2005) 19560–19562.
[40] N. Roy, Y. Sohn, D. Pradhan, ACS Nano 7 (2013) 2532–2540.
[41] J. Pan, G. Liu, G.Q. Lu, H.M. Cheng, Angew. Chem. Int. Ed. 50 (2011) 2133–2137.
[42] H. Zhang, Y. Wang, P. Liu, Y. Han, X. Yao, J. Zou, H. Cheng, H. Zhao, A.C.S. Appl, Mater. Interfaces 3 (2011) 2472–2478.
[43] Y. Luan, L. Jing, Y. Xie, X. Sun, Y. Feng, H. Fu, ACS Catal. 3 (2013) 1378–1385.
[44] M. Chen, J. Ma, B. Zhang, G. He, Y. Li, C. Zhang, H. He, Appl. Catal. B 207 (2017) 397–403.
[45] M. Bellardita, C. Garlisi, A.M. Venezia, G. Palmisano, L. Palmisano, Catal. Sci. Technol. 8 (2018) 1606–1620.
[46] M. Maisano, M.V. Dozzi, M. Coduri, L. Artiglia, G. Granozzi, E. Selli, A.C.S. Appl, Mater. Interf. 8 (2016) 9745–9754.
[47] H. Tong, Y. Zhou, G. Chang, P. Li, R. Zhu, Y. He, Appl. Surf. Sci. 444 (2018) 267–275.
[48] S. Bai, L. Wang, Z. Li, Y. Xiong, Adv. Sci. 4 (2017) 1600216.
[49] Z. Wang, K. Lv, G. Wang, K. Deng, D. Tang, Appl. Catal. B 100 (2010) 378–385.
[50] J.C. Yu, J. Yu, W. Ho, Z. Jiang, L. Zhang, Chem. Mater. 14 (2002) 3808–3816.
[51] E.M. Samsudin, S.B.A. Hamid, J.C. Juan, W.J. Basirun, A.E. Kandjani, S.K. Bhargava, Appl. Surf. Sci. 365 (2016) 57–68.
[52] M.V. Dozzi, L. Artiglia, G. Granozzi, B. Ohtani, E. Selli, J. Phys. Chem. C 118 (2014) 25579–25589.
[53] Q. Xiang, K. Lva, J. Yu, Appl. Catal. B 96 (2010) 557–564.
[54] M. Minella, M.G. Faga, V. Maurino, C. Minero, E. Pelizzetti, S. Coluccia, G. Martra, Langmuir 26 (2010) 2521–2527.
[55] H. Park, W. Choi, J. Phys. Chem. B 108 (2004) 4086–4093.
[56] A.M. Czoska, S. Livraghi, M. Chiesa, E. Giamello, S. Agnoli, G. Granozzi, E. Finazzi, C. Di Valentin, G. Pacchioni, J. Phys. Chem. C 112 (2008) 8951–8956.
[57] K. Lv, B. Cheng, J. Yu, G. Liu, Phys. Chem. Chem. Phys. 14 (2012) 5349–5362.
[58] J. Song, H.B. Yang, X. Wang, S.Y. Khoo, C.C. Wong, X.-W. Liu, C.M. Li, A.C.S. Appl, Mater. Interf. 4 (2012) 3712–3717.
[59] B. Choudhury, A. Choudhury, Int. Nano Letter. 3 (2013) 55.
[60] J. Zhu, S. Wang, Z. Bian, S. Xie, C. Cai, J. Wang, H. Yang, H. Li, Cryst. Eng. Comm. 12 (2010) 2219–2224.
[61] X. Hu, S. Lu, J. Tian, N. Wei, X. Song, X. Wang, H. Cui, App. Catal. B 241 (2019) 329–337.
[62] A. Di Paola, G. Cufalo, M. Addamo, M. Bellardita, R. Campostrini, M. Ischia, R. Ceccato, L. Palmisano, Colloid Surfaces A 317 (2008) 366–376.
[63] A. Di Paola, M. Bellardita, R. Ceccato, L. Palmisano, F. Parrino, J. Phys. Chem. C 113 (2009) 15166–15174.
[64] Q. Wang, C. Chen, D. Zhao, W. Ma, J. Zhao, Langmuir 24 (2008) 7338–7345.
[65] J.G. Yu, W.G. Wang, B.L. Su, J. Phys. Chem. C 113 (2009) 6743–6750.
[66] J.C. Parker, R.W. Siege, Appl. Phys. Lett. 57 (1990) 943–945.
[67] Q. Zhu, Y. Peng, L. Lin, C.M. Fan, G.Q. Gao, R.X. Wang, A.W. Xu, J. Mater. Chem. A 2 (2014) 4429–4437.
[68] G. Liu, H.G. Yang, X. Wang, L. Cheng, H. Lu, L. Wang, G.Q. Lu, H.M. Cheng, J. Phys. Chem. C 113 (2009) 21784–21788.
[69] J. Liqiang, Q. Yichun, W. Baiqi, L. Shudan, J. Baojiang, Y. Libin, F. Wei, F. Honggang, S. Jiazhong, Sol. Energ. Mat. Sol. C. 90 (2006) 1773–1787.
[70] O. Pikuda, C. Garlisi, G. Scandura, G. Palmisano, J. Catal. 346 (2017) 109–116.
[71] J. Liu, J. Li, A. Sedhain, J. Lin, H. Jiang, J. Phys. Chem. C 112 (2008) 17127–17132.
[72] T.C. Jagadale, S.P. Takale, R.S. Sonawane, H.M. Joshi, S.I. Patil, B.B. Kale, S.B. Ogale, J. Phys. Chem. C 112 (2008) 14595–14602.
[73] H.R.S. Abdellatif, G. Zhang, X. Wang, D. Xie, J.T.S. Irvine, J. Ni, C. Ni, Chem. Eng. J. 370 (2019) 875–884.
[74] K. Lv, J. Yu, K. Deng, X. Li, M. Li, J. Phys. Chem. Solid. 71 (2010) 519–522.
[75] U. Alam, A. Khan, D. Ali, D. Bahnemann, M. Muneer, RSC Adv. 8 (2018) 17582–17594.
[76] M.C. Biesinger, L.W.M. Lau, A.R. Gerson, R. St, C.W. Smart, Appl. Surf. Sci. 257 (2010) 887–898.
[77] S. Haukka, E.L. Lakomaa, O. Jylha, J. Vilhunen, S. Hornytzkyj, Langmuir 9 (1993)

[78] N. Aas, T.J. Pringle, M.J. Bowker, Chem. Soc. Faraday Trans. 90 (1994) 1015–1022.
[79] J.G. Li, R. Buchel, M. Isobe, T. Mori, T. Ishigaki, J. Phys. Chem. C 113 (2009) 8009–8015.
[80] Y. Ma, H.D. Asfaw, C. Liu, B. Wei, K. Edström, Nano Energy 30 (2016) 745–755.
[81] G. Cao, Y. Li, Q. Zhang, H. Wang, J. Hazard. Mater. 178 (2010) 440–449.
[82] T. Rajh, N.M. Dimitrijevic, M. Bissonnette, T. Koritarov, V. Konda, Chem. Rev. 114 (2014) 10177–10216.
[83] A. Di Paola, M. Bellardita, B. Megna, F. Parrino, L. Palmisano, Catal. Today 252 (2015) 195–200.
[84] F. Zuo, L. Wang, T. Wu, Z. Zhang, D. Borchardt, P. Feng, J. Am. Chem. Soc. 132 (2010) 11856–11857.